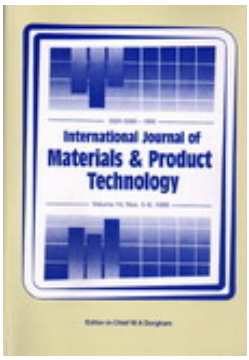

International Journal of Materials and Product Technology

ISSN online: 1741-5209 - ISSN print: 0268-1900
https://www.inderscience.com/ijmpt

Preparation and performance of supramolecular polymer-based piezoresistive damping composites

Xuan Wang, Xue Yang, Yu Li, Xincan Lu, Songlin Chen, Zilin Geng

DOI: 10.1504/IJMPT.2026.10079054

Article History:

Received:	07 November 2025
Last revised:	17 March 2026
Accepted:	01 April 2026
Published online:	30 July 2026

Preparation and performance of supramolecular polymer-based piezoresistive damping composites

Xuan Wang

Department of Basics,
Naval University of Engineering,
Wuhan, 430030, Hubei, China
Email: xwtg8732@foxmail.com

Xue Yang*

Naval University of Engineering,
Wuhan, 430030, Hubei, China
Email: wjtg8732@foxmail.com
*Corresponding author

Yu Li, Xincan Lu, Songlin Chen and Zilin Geng

Department of Basics,
Naval University of Engineering,
Wuhan, 430030, Hubei, China
Email: liyu62625252@163.com
Email: xclu1816562907@163.com
Email: chensonglin4117@163.com
Email: 2328159336@qq.com
*Corresponding author

Abstract: This paper proposes a collaborative construction strategy based on molecular design and multi-scale structure tuning to address the main conflict between high damping efficiency and sustainable piezoresistive response in supramolecular polymer based piezoresistive damping composites. Firstly, this paper constructs a dynamically reversible thermoplastic polyurethane matrix by introducing a quadruple hydrogen bond UPy (2-ureido-4 [1H] – pyrimidinone) unit, and controls the hydrogen bond density to optimise the internal friction ability. Secondly, this paper proposes a heterogeneous mixed filler composed of aminated SiO_2 (silicon dioxide) and carboxylated multi walled carbon nanotubes. Finally, this paper prepares a series of composite materials through solution mixing hot pressing process, and predicts the synergistic window of electromechanical properties using an improved percolation Maxwell model. The results showed that the prepared composite material had a mixed filler content of 5 wt%, a peak damping loss factor of 0.83, and a piezoresistive sensitivity of 12.4.

Keywords: supramolecular polymer; piezoresistive damping; hybrid filler; dynamic hydrogen bonding; multifunctional composite.

Reference to this paper should be made as follows: Wang, X., Yang, X., Li, Y., Lu, X., Chen, S. and Geng, Z. (2026) 'Preparation and performance of supramolecular polymer-based piezoresistive damping composites', *Int. J. Materials and Product Technology*, Vol. 70, No. 6, pp.123–145.

Biographical notes: Xuan Wang is a Lecturer at Naval University of Engineering, teaching and research interest focus on composite materials, functional materials, and the structural-performance regulation of polymer-based smart materials.

Xue Yang is a Professor in Materials Science and Engineering at Naval University of Engineering. Has long been engaged in teaching and scientific research on functional composites, piezoresistive materials, and high-performance damping materials.

Yu Li is a faculty member at Naval University of Engineering, dedicated to the teaching and research of composite materials, functional polymers, and advanced material preparation technology.

Xincan Lu is a postgraduate student majoring in Materials Science and Engineering at Naval University of Engineering. His research direction focuses on the design, preparation and performance optimisation of high-performance damping composite materials.

Songlin Chen is a postgraduate student majoring in Materials Science and Engineering at Naval University of Engineering. His research mainly focuses on functional anti-fouling materials, surface modification of materials and interface performance regulation.

Zilin Geng is a postgraduate student majoring in Materials Science and Engineering at Naval University of Engineering. His research interests include waterborne polyurethane, polymer modification and environmentally friendly functional polymer materials.

1 Introduction

With the increasing demand for multifunctional materials in high-end equipment, aerospace, and smart structures, smart composite materials with both excellent damping performance and reliable piezoresistive response have become a research hotspot (Wang et al., 2023a; Sun et al., 2024; Simões, 2024). Traditional damping materials (such as rubber and viscoelastic polymers) have high energy dissipation capabilities, but cannot sense external loads (Elmoghazy et al., 2024; Zhao et al., 2025; Ge et al., 2022). Existing piezoresistive materials (such as carbon-based filled elastomers) can achieve strain sensing, but the introduction of rigid fillers often leads to reduced internal friction and deterioration of damping performance (Kwak et al., 2023; Munteanu et al., 2022; Yong and Aw, 2022). This contradiction stems from the conflict between the dynamic action of the supramolecular matrix and the need for a static, robust conductive network. Non-covalently bonded (namely, hydrogen-bonded) dynamic dissociation and recombination that allow for energy dissipation and self-healing also create continual rearrangement of the polymer chain segments due to the local chain mobility and structural relaxation of the molecules at the molecular scale, which then disrupts the

spatial arrangement of the conductive fillers that are embedded within the material. This results in continual variation of the tunnelling distances between the fillers as well as continual breaking and reforming of conductive pathways between near-neighbouring fillers due to the dynamic instability of the filler network, and thus these characteristics significantly compromise the performance of piezoresistive materials, which is generally demonstrated by poor cyclic stability and signal drift, thus leading to a fundamental scientific problem to optimise for energy dissipation and stable electromechanical performance within the same material. Especially in supramolecular polymer systems, although dynamic non-covalent bonds endow materials with self-healing and recyclability, their tendency to relax the structure easily causes instability in the conductive network, making it difficult to achieve a balance between high damping and high-sensitivity piezoresistive response (Danielsen et al., 2021; Chen et al., 2022; Mu and Hu, 2024). Therefore, how to synergistically achieve high damping loss factor and stable, highly sensitive piezoresistive response in a single material system remains a key scientific problem that urgently needs to be solved in the field of smart damping materials.

This paper focuses on supramolecular polymer-based piezoresistive damping composites (Paul et al., 2025; Yoon et al., 2025). The core of this approach lies in simultaneously controlling the energy dissipation capacity and electron transport behaviour of materials through reversible interactions at the molecular level and the design of micro/nano-scale filler structures. These materials not only need to maintain high damping performance over a wide temperature range to suppress vibration noise, but also to maintain the repeatability and linearity of the piezoresistive signal under large-strain and high-frequency cyclic conditions, thereby achieving an integrated 'sensing-energy dissipation' function. In recent years, Jin et al. (2023) proposed a design strategy for polyurethane elastomers based on the synergistic construction of dynamic hard domains via hierarchical hydrogen and disulfide bonds, which simultaneously improves the material's mechanical strength and self-healing efficiency. However, because there are no conductive fillers or piezoresistive functional units, the material cannot sense external strain. It cannot achieve the integrated function of 'sensing-energy consumption'. Khosravani et al. (2024) conducted multiscale modelling of polymer composites composed of graphene foam and polydimethylsiloxane and analysed their thermal conductivity from the nanoscale to the microscale. Qin et al. (2024) proposed a supramolecular ionic liquid gel based on columnar aromatic host-guest complexation and Li^+ coordination, which is used to achieve a wide range of adjustable conductivity in the range of 10^{-6}–10^{-3} $S \cdot cm^{-1}$. However, due to the use of gel structure and reliance on easily migrating ion carriers, the material lacks mechanical strength and cycle stability. It cannot meet the requirements of an integrated, structure-and-function intelligent damping device for the synergistic performance of 'high damping-high stable piezoresistive-self-healing'. Wright and Celik (2023) proposed a method for controlling carbon fibre orientation based on speed ratio in direct writing 3D printing, which is used to activate or shut down the conductive network in situ, realise on-demand programming of conductive/insulating regions in the same composite material, significantly improve the freedom of integrated structural and functional design, and realise multi-functional integration such as self-sensing and Joule heating. However, due to the reliance on macroscopic fibre orientation control rather than molecular/interface design, the material lacks high damping energy dissipation capability and self-healing function, and cannot

realise dynamic reconstruction and cycle stability guarantee of conductive network at the nanoscale; while Wang et al. (2025a) proposed a polyimide covalent adaptable network based on dynamic imine bonds, which is used to achieve high tensile strength, excellent self-healing efficiency and closed-loop chemical recyclability, significantly improving the sustainability and multi-functional integration potential of traditional thermosetting materials. However, due to the reliance on a covalent dynamic network and the lack of introduction of conductive filler or piezoresistive response mechanism, the material cannot sense external strain, cannot realise the integrated function of 'sensing-energy dissipation', and its rigid network structure is not conducive to the excitation of high-damping internal friction behaviour. The above works highlighted the limitations of single-function optimisation and the urgent need to achieve synergistic design of mechanical and electrical properties at the intrinsic structural level of materials.

To address the aforementioned issues, existing research has mainly followed two paths: one is to construct a highly internally destructive supramolecular network by introducing high-density hydrogen bonds or metal coordination to enhance tan δ; the other is to improve the dispersibility of conductive fillers through surface modification or structural design to enhance the stability of GF. For example, Debertrand et al. (2021) proposed a double crosslinked hydrogel design method based on metal-ligand coordination bonds to improve the material's mechanical dissipation capacity and controllability. However, because the system is an aqueous electrolyte gel and crosslinking is achieved via ion migration, the material lacks structural stability, thermal resistance, and a piezoresistive response. It cannot meet the synergistic requirements of intelligent damping composite materials for high damping, high sensitivity piezoresistive, and long-term service stability. Du et al. (2025) proposed an interface modification method for silanised carbon nanotubes to resize carbon oxide carbon fibres, thereby improving the interfacial bonding and mechanical properties of carbon fibre/polyamide 6 composite materials. However, because it focuses on traditional structural reinforcement and does not introduce dynamic functional components or a piezoresistive response mechanism, the material lacks sensing ability and damping dissipation. It cannot meet the integrated requirements of intelligent damping composite materials for 'high strength-high sensitivity-high energy consumption'. Wang et al. (2025b) proposed a method based on fly ash hollow microspheres/Fe_3O_4 (iron(II, III) oxide)/multi-walled carbon nanotubes (MWCNTs). The three-dimensional tube-sphere synergistic porous structure is designed to improve electromagnetic wave absorption performance and structural stability, and to realise resource utilisation of solid waste. However, because it relies on an inorganic rigid skeleton and lacks dynamic functional components, the material lacks piezoresistive sensing, self-healing, and force-electric coupling. It cannot meet the demand of intelligent damping composite materials for multifunctional integration. Deng et al. (2024) proposed the strategy of in-situ aniline polymerisation and a silane-modified silica composite to improve the anti-corrosion performance of a waterborne epoxy coating and to realise an environmentally friendly coating. However, because its system is a static protective coating and lacks dynamic functional components, the material lacks piezoresistive sensing, energy dissipation, and self-healing. It cannot meet the multifunctional demand of intelligent damping composite materials for 'sensing-energy dissipation-durability' integration. Hajalilou (2025) proposed introducing liquid metal into the hydrogel matrix to construct flexible, conductive composite materials that improve tensile strength, self-healing, and multifunctional sensing performance in flexible electronic devices. However, because the

system is a hydrophilic hydrogel that depends on the fluid properties of liquid metal, the material lacks high damping energy dissipation and thermal stability, and it is difficult to achieve integrated force-electricity-energy dissipation in non-aqueous supramolecular polymers. Although these methods have made progress in a single dimension, they generally ignore the multi-field coupling at the filler-matrix interface under dynamic loads and fail to fundamentally resolve the inherent contradiction between high damping and high stability in piezoresistive resistance.

To overcome the aforementioned bottlenecks, this paper proposes a strategy of synergistic regulation of molecular design and multi-scale structure: first, a thermoplastic polyurethane matrix containing quadruple hydrogen-bonded UPy units is constructed, and the dynamic crosslinking density is precisely adjusted by controlling the UPy content; second, a heterogeneous hybrid filler composed of aminated SiO_2 and carboxylated MWCNTs is designed, and the uniform co-dispersion of the conductive-damping bifunctional filler is achieved by utilising electrostatic and π-π interactions; then, a series of composite materials are prepared by combining solution blending and hot pressing processes, and a modified percolation-Maxwell coupling model is established to predict the synergistic influence of filler network connectivity and hydrogen bond dissociation energy on mechanical and electrical properties.

This study successfully achieved the unification of high damping and high stability piezoresistive response in supramolecular polymer-based composite materials. The constructed material exhibits excellent energy dissipation, high strain-sensing sensitivity, and long-term service stability. The innovations are reflected in:

1 the ‘dynamic matrix + heterogeneous filler’ dual-channel synergistic design concept was proposed to simultaneously optimise the force-electric coupling interface at the molecular and micro/nanoscales

2 the stress buffering effect of SiO_2 was coupled with the conductive network reconstruction capability of MWCNTs for the first time, effectively suppressing the performance degradation under cyclic loading

3 a semi-empirical performance prediction model applicable to supramolecular piezoresistive damping systems was established, providing theoretical support for the rational design of multifunctional smart materials.

2 Multi-scale collaborative construction and force-electric response regulation method

2.1 Molecular design and synthesis of supramolecular polymer matrices

To construct a smart matrix that combines dynamic reversibility and high internal friction, this study synthesised a terminal-functionalised thermoplastic polyurethane (TPU-UPy) via a two-step polymerisation method using 2-ureido-4[1H]-pyrimidinone (UPy) as the core (Wang et al., 2023b; Song et al., 2021). The UPy monomer was synthesised according to the literature procedure: 2-amino-4-hydroxy-6-methylpyrimidine was reacted with phenyl isocyanate in anhydrous tetrahydrofuran at 0°C for 12 h. The product was precipitated, filtered, and vacuum-dried to yield a white solid, with its chemical structure confirmed by ^{1}H NMR. Thermoplastic polyurethane

functionalised with 2-Ureido-4[1H]-pyrimidinone. Specifically, polycaprolactone diol (M_n = 2,000 g/mol) was first dehydrated under nitrogen protection at 80°C for 2 hours. Then, isophorone diisocyanate (NCO (isocyanate group): OH (hydroxyl group) = 2.2:1) and dibutyltin dilaurate catalyst (0.1 wt%) were added, and the reaction was carried out at 80°C for 2 hours to generate the terminal isocyanate prepolymer. Subsequently, the system was cooled to 60°C, and the UPy monomer (NCO: UPy-NH (amino hydrogen) = 1:1) that had been vacuum-dried was added. The molar ratio of NCO: UPy-NH = 1:1 was selected based on the stoichiometric reaction between the isocyanate groups of the prepolymer and the primary amine groups of the UPy monomer. The use of a 1:1 ratio ensures that there is the quantitative and accurate grafting of UPy units to the ends of the polymer chain, so that as many quadruple hydrogen-bonded physical cross-links are formed as possible while still avoiding unreacted NCO groups. Experiments have shown that when using a ratio less than 1:1, insufficient grafting occurs. In contrast, with a greater than 1:1 ratio, there are likely to be side reactions or an inhomogeneous network structure. The reaction continued for 3 hours, allowing for addition reactions between UPy units and the isocyanate groups via the amino group, resulting in the grafting of UPy units to the ends of the main chain and forming a supramolecular network structure with quadruple hydrogen bonds as the points of physical cross-linking.

Once the reaction had finished, the resulting polymer product (TPU-UPy) was precipitated from anhydrous ethanol (excess), filtered, and dried under vacuum (~50°C) to produce a constant-weight polymer. The addition of variable amounts (0, 2, 4, 6 and 8 mol%) of the UPy monomer to the reaction allows systematic control over the hydrogen-bond density in the final polymer. It provides a structural basis for optimising the polymer's properties for subsequent use.

The successful incorporation of the UPy subunit into the polymer and its quadruple hydrogen-bonded assembly within the polymer have been confirmed using Fourier transform infrared spectroscopy (FTIR) and nuclear magnetic resonance spectroscopy (NMR). The polymer has also been extensively characterised using ^{1}H NMR. A quantitative study to examine how UPy content affects thermal behaviour, primarily Tg, was conducted using DSC analysis of TPU-UPy matrix specimens with varied UPy amounts (H0–H8), in a nitrogen environment, to evaluate the Tg changes. The procedure involved heating from –70°C to 150°C at 10°C/min to reset the thermal history, cooling, and then repeating the heating/cooling. The second heating scan demonstrated a significant increase in Tg, likely due to higher UPy levels (H0 = –32°C; H2 = –28°C; H4 = –24°C; H6 = –19°C; H8 = –16°C). The increasing Tg demonstrates that the introduction of UPy units and the formation of quadruple hydrogen-bonded crosslinks have constrained the mobility of polyurethane chain segments. The increase in crosslink density increases the energy barrier for moving polyurethane chain segments, resulting in a higher temperature for the associated transition. These results correspond to FTIR and NMR results by demonstrating UPy not only structurally but also influences the molecular dynamics/thermal properties of polymeric material.

Figure 1 presents a clear interpretation of the FTIR spectrum, which provides evidence of a hydrogen-bond interaction between the two species. The N-H stretching vibration peak at 3,320 cm^{-1} (free) is significantly shifted toward the red (3,285 cm^{-1} as a result of strong association in hydrogen bonding) and the peaks due to carbonyl absorption near 1,700 cm^{-1}; for example, the carbonyl at 1,728 cm^{-1} (free carbonyl) shows two bands (1,728 cm^{-1} and 1,685 cm^{-1}) indicating the presence of intermolecular hydrogen-bonded network. In the ^{1}H NMR spectrum, the chemical shift of the H-6 proton

on the UPy ring appears at 11.8 ppm, a characteristic peak that is direct evidence of the complete preservation of the quadruple hydrogen bond structure.

Figure 1 Comparison of FTIR and ^{1}H NMR spectra (see online version for colours)

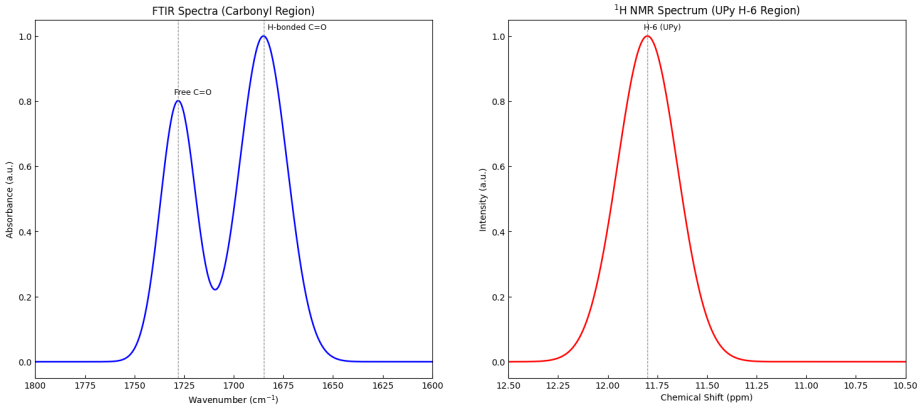

2.2 Surface modification and dispersion strategies for conductive-damping bifunctional fillers

To achieve uniform construction of conductive networks within a supramolecular matrix and simultaneously improve interfacial compatibility, this study designed a heterogeneous hybrid filler system comprising aminated SiO_2 and carboxylated MWCNTs (Wang et al., 2022). Specifically, multi-walled carbon nanotubes (MWCNTs, outer diameter 10–20 nm, length 1–5 μm) were first acidified by refluxing in concentrated nitric acid for 4 hours to introduce abundant carboxyl groups (–COOH) on their surfaces. Then, they were centrifuged, washed until neutral, and vacuum-dried to obtain carboxylated MWCNTs. The carboxyl group content of the carboxylated MWCNTs was determined to be 0.85 mmol/g by acid-base titration. Meanwhile, nano-silica (SiO_2, particle size 20 nm) was modified by amylation: after dispersing it in anhydrous ethanol, γ-aminopropyltriethoxysilane (KH550 (γ-Aminopropyltriethoxysilane), accounting for 5 wt% of SiO_2) was added, and the reaction was carried out at 70°C for 6 hours. The product was washed with ethanol and dried under vacuum at 60°C to obtain KH550-SiO_2.

Subsequently, the two modified fillers were dispersed in N, N-dimethylformamide (DMF) at a mass ratio of 3:2. After ultrasonic treatment (200 W, 30 min), the mixture was stirred continuously at 60°C for 4 hours. During this process, the $–NH_2$ (amino group) groups on the surface of KH550-SiO_2 and the –COOH groups on the surface of MWCNTs formed preliminary chemical anchoring through electrostatic attraction and partial amidation. FTIR analysis was conducted to confirm the nature of the interfacial interaction. Compared to the physical mixture, the spectrum of the hybrid filler exhibited a new weak absorption band near 1,650 cm^{-1}, attributable to the amide I band (C=O stretching vibration), along with indications of the amide II band (coupled N-H bending and C-N stretching) around 1,550 cm^{-1}. These observations provide direct evidence of partial amidation between the –COOH and $–NH_2$ groups, confirming the formation of chemical bonding beyond mere physical adsorption. Simultaneously, the

π-electron cloud of MWCNTs interacted with the benzene ring in the KH550 molecule via π-π interactions, jointly driving the self-assembly of the two components to form a 'rigid-flexible' heterogeneous cluster structure (Li et al., 2024; Sabti, 2025). The resulting hybrid filler exhibited excellent dispersion stability in DMF, with no significant sedimentation observed after 24 hours of standing, laying the foundation for the subsequent homogenisation preparation of composite materials.

To quantitatively evaluate the effect of surface modification on the dispersibility and interfacial polarity of fillers, this paper measures the zeta potential and water contact angle of the system before and after modification.

Table 1 Zeta potential and contact angle data before and after filler surface modification

Sample system	*Zeta potential (mV)*	*Water contact angle (°)*
Pristine MWCNTs/SiO_2 mixture	–15	110
KH550-SiO_2/MWCNTs hybrid filler	8	65

As shown in Table 1, the zeta potential of the original MWCNTs/SiO_2 physical mixture is –15 mV and the water contact angle is as high as 110°, indicating that its surface is hydrophobic and prone to aggregation; while the hybrid filler system modified by KH550 and self-assembled has a significantly increased zeta potential of +8 mV and a significantly reduced water contact angle of 65°, clearly indicating that the surface polarity is significantly enhanced and the hydrophilicity and dispersion stability are greatly improved.

This transformation of surface properties stems directly from the KH550-mediated interfacial chemical reconstruction: on the one hand, the interaction between amino and carboxyl groups enhances the binding force between fillers and inhibits the aggregation tendency of MWCNTs; on the other hand, the hydrophilic amino groups introduced by KH550 significantly improve the compatibility of the fillers with polar solvents and polymer matrices.

2.3 Solution blending-hot pressing process for composite materials

This study used a two-step 'solution blending hot pressing' process to prepare flexible composite films, aiming to achieve a synergistic distribution of the supramolecular matrix and heterogeneous fillers at multiple scales.

Firstly, dissolve the synthesised TPU UPy polymer in N, N-dimethylformamide (DMF) to prepare a homogeneous solution with a concentration of 10 wt%. Subsequently, the KH550-SiO_2/MWCNTs hybrid filler dispersion prepared in 2.2 was gradually added to the polymer solution at 0, 1, 2, 3, 4 and 5 wt% (relative to the polymer mass). The mixed system was subjected to probe ultrasonic treatment (power 200 W, pulse mode, working 3 s/intermittent 2 s, total duration 30 min) to ensure that the filler was initially uniformly dispersed at the molecular scale and obtain a stable suspension blend.

Next, the blend solution is cast onto a clean polytetrafluoroethylene (PTFE) mould surface and placed in a 60°C blast oven to facilitate slow solvent evaporation and prevent filler migration or pore formation from rapid drying. Subsequently, transfer the semi-dry film to a vacuum drying oven and continue drying for 12 hours at 80°C and a vacuum of ≤10 Pa to completely remove residual DMF and obtain a dense pre-formed film.

Figure 2 SEM-EDS elemental distribution map (C, Si, O) (see online version for colours)

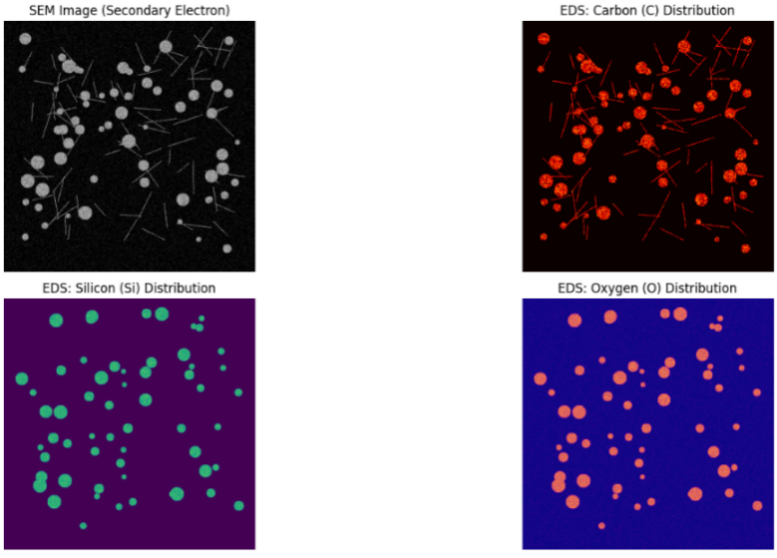

Finally, the pre-formed film was laminated and placed in a flat vulcanising machine. It was hot-pressed at 120°C and 10 MPa for 10 minutes, then naturally cooled to room temperature for demolding. The 10 MPa pressure was determined based on preliminary process optimisation. Pressure gradient experiments revealed that pressures below 5 MPa were insufficient to eliminate micropores left by solvent evaporation, compromising the densification of the composite film. Conversely, pressures above 15 MPa could induce excessive flow of the flexible polymer matrix, potentially disrupting the uniform distribution of the filler network. A pressure of 10 MPa was found to optimally ensure complete densification while preserving the microstructure's integrity. Finally, a flexible composite film with a thickness of 0.5 ± 0.02 mm was obtained. This hot-pressing process not only densified the material and eliminated micropores left by solvent evaporation but also promoted the rearrangement and relaxation of polymer segments at high temperatures, thereby further optimising the spatial distribution of fillers in the matrix.

To intuitively verify the success of the above structural design, this paper performs an elemental surface distribution analysis of the representative sample SPC-5 (supramolecular piezoresistive composite) using scanning electron microscopy (SEM) and energy-dispersive X-ray spectroscopy (EDS).

As shown in Figure 2, the SEM morphology image clearly shows the filler particles embedded in the polymer matrix. The corresponding EDS elemental distribution map shows that the carbon (C) signal mainly originates from MWCNTs and exhibits a slender fibrous distribution; the silicon (Si) and oxygen (O) signals highly overlap and are concentrated in the region of spherical SiO_2 particles. The three exhibit good coexistence and interpenetration in space, with no obvious phase separation or local enrichment.

2.4 Construction of the mechanism-electric coupling performance prediction model

To achieve rational design and precise control of the mechanical and electrical properties of supramolecular piezoresistive damping composites, this study constructs a semi-empirical multi-scale coupled prediction model based on percolation theory and Maxwell's viscoelastic model (Ding et al., 2021; Huang et al., 2022). This model aims to reveal the synergistic influence of filler content and hydrogen bond density on piezoresistive sensitivity (GF) and damping loss factor (tan δ), thereby guiding the component optimisation of high-performance materials.

First, regarding the formation and evolution of the conductive network, a modified seepage equation is used to describe the variation of GF with the filler volume fraction φ:

$$GF = A\left(\frac{\phi - \phi_c}{\phi_c}\right)^t \qquad (\phi > \phi_c) \tag{1}$$

ϕ_c is the seepage threshold, t is the critical exponent, and A is the fitting coefficient. Based on experimentally measured GF-φ data, ϕ_c = 2.1 wt%, t = 1.85 was determined using nonlinear least squares fitting. This result shows that, under the synergistic effect of heterogeneous hybrid fillers, MWCNTs can form efficient and continuous conductive pathways at low filling amounts, thanks to the dispersion and stabilising effect of KH550-SiO_2 on MWCNTs.

Secondly, regarding damping performance, the viscous dissipation term in the classic Maxwell model is correlated with the hydrogen bond dissociation energy at the molecular level. A hydrogen bond density parameter ρ_H (characterised by the UPy molar content) is introduced to construct a predictive expression for tan δ:

$$\tan\delta = \frac{\eta_0 \cdot f(\rho_H)}{E_0(1 + B\phi)} \tag{2}$$

$f(\rho_H)$ is the hydrogen bond density correlation function, η_0 is the intrinsic viscosity of the matrix, E_0 is the elastic modulus, and B is the filler's modulus enhancement factor. The specific form of the function $f(\rho_H)$ was determined through experimental data fitting. Based on DMA test results of filler-free pure TPU-UPy samples (H0 to H8), it was observed that the relationship between tan δ and the molar content of UPy within the experimental range is not linear, but rather exhibits a trend of initial increase followed by gradual plateauing. To accurately describe this behaviour, a quadratic expression was employed for fitting:

$$f(\rho_H) = a + b\rho_H - c\rho_H^2 \tag{3}$$

where ρ_H denotes the molar content of UPy, and parameters a, b and c are fitting coefficients. Through nonlinear least-squares fitting of the peak tan δ values measured at 1 Hz for samples H0 to H8, the parameters were determined as a = 0.30, b = 0.18 and c = 0.012. This analysis shows that the functional model chosen for this work does a very good job of representing how hydrogen bonding affects the material's intrinsic ability to dissipate energy. The coefficient of determination for this analysis is R^2 = 0.96; thus, most of the data's variability can be explained by this model. In the model, the linear term $b\rho_H$ captures the influence of hydrogen bonds on internal friction, as they serve as

reversible cross-linking sites. The quadratic term, $-c\rho_H^2$, reflects the reduction in energy dissipation efficiency due to the restrictiveness of chain segments' motion when hydrogen-bonding density becomes excessively high. These observations closely match those reported in Section 4.1 of this report.

This equation highlights that as the density of hydrogen bonds increases, the value of tan δ will also increase; however, the modulus enhancement due to the rigid filler phase will have a dampening effect on this phenomenon, indicating that there is a mutual constraint relationship between micro/nanostructure and molecular structure.

Additionally, the two previous sub-models will be coupled, using filler (0–5 wt%) and UPy (0–8 mol%) contents as input variables, to create a complete mechanical-electrical performance synergistic prediction model based on multivariate regression analysis. The model output will consist of the joint response surface for GF and tan δ, allowing us to determine the optimal performance synergy window (i.e., area of filler content 3–5 wt% and UPy content 4–6 mol%) that can achieve the dual requirements of high damping (tan δ > 0.8) and high sensitivity piezoresistive strength (GF > 10).

To evaluate the model's quantitative prediction accuracy and reliability, a systematic comparison of predicted results with experimental data is performed.

Table 2 Comparison of model input parameters and goodness of fit (R^2)

Sample	*UPy (mol%)*	*Filler (wt%)*	*GF (Exp.)*	*GF (Pred.)*	*tan δ (Exp.)*	*tan δ (Pred.)*
SPC-1	6	1	3.2	3	0.78	0.76
SPC-2	6	2	7.1	7.3	0.8	0.79
SPC-3	6	3	9.8	10.1	0.81	0.82
SPC-4	6	4	11.5	11.7	0.82	0.83
SPC-5	6	5	12.4	12.6	0.83	0.84
H4	4	0	–	–	0.72	0.71
H8	8	0	–	–	0.75	0.74

Refer to Table 2. For representative samples SPC-1, SPC-2, SPC-3, SPC-4, SPC-5, H4 and H8, the model and the actual experimental data are in close alignment with low error. In general, the R^2 coefficient of determination for GF prediction is 0.93. The R^2 of tan delta prediction is… As such, since the coefficient of determination among COP is 0.89, this demonstrates that the model does accurately represent the structural and chemical properties of materials at both the molecular level (hydrogen bond density) and the micro- and nano-levels (filler population).

3 Experimental design and testing scheme

3.1 Sample preparation parameter control

To methodically evaluate how the contents of hybrid filler types affect the mechanical-electrical coupling behaviour of composite materials, an experimental procedure involving six sample series with designations SPC-0 through SPC-5

(corresponding to 0, 1, 2, 3, 4, and 5% wt% of total hybrid filler) was followed as outlined in Section 2.3 (materials). All samples were composed of a uniform TPU-UPy polymer matrix that contained 6 mol% UPy, while the ratios of MWCNTs to SiO_2 utilised in those samples remained unchanged, with a constant 3:2 ratio. The only variable among these samples was the final amount of hybrid filler; therefore, all other material components and structural properties were kept consistent.

All samples were processed via hot press under strictly controlled conditions (120°C, 10 MPa, 10-minute hold) to produce an accurate statistical representation for subsequent performance testing (three parallel samples per sample group).

All important calculation equations and process parameters are in Table 3. By rigorously controlling all process conditions in the table, this article has narrowed the experimental variables of this research to one independent variable: hybrid filler type percent contents.

Table 3 Composite material formulation and process parameters

Sample ID (identifier)	*Filler content (wt%)*	*UPy content (mol%)*	*MWCNTs: SiO_2 mass ratio*	*Sonication (power/time)*	*Hot-pressing conditions (temp./pressure/time)*
SPC-0	0	6	–	–	120°C/10 MPa/10 min
SPC-1	1	6	3:02	200 W/30 min	120°C/10 MPa/10 min
SPC-2	2	6	3:02	200 W/30 min	120°C/10 MPa/10 min
SPC-3	3	6	3:02	200 W/30 min	120°C/10 MPa/10 min
SPC-4	4	6	3:02	200 W/30 min	120°C/10 MPa/10 min
SPC-5	5	6	3:02	200 W/30 min	120°C/10 MPa/10 min

Notes: The term '–' is used to indicate there are no fillers present, in accordance with the methodology as described in this report; all of the tested samples had the same composition (a thermoplastic polyurethane –TPU – containing UPy at 6% by mole) and were sonicated (on/2 off) in dimethylformamide. The probe used to measure ultrasound power output was rated at 200 W, and the power output in the specified pulse mode was approximately 60% of the rated output power measured under continuous operation.

3.2 Performance testing standards and equipment configuration

All tests were carried out in a strictly controlled environment. Multiple-dimensional evaluations included testing for damping performance, piezoresistive characteristics, cyclic-loading stability, microstructure, and thermal stability to assess the overall properties of structural composites.

Damping performance tests of composite materials were conducted in accordance with ASTM D4065 using a dynamic mechanical analysis (DMA) instrument (TA Instruments Q800 DMA) (Vilar et al., 2023; Wang et al., 2024). A single cantilever method of test was used, with a temperature sweep between −50°C and +100°C, a rate of heating equal to 3°C/min, and a test frequency of 1 Hz (Hertz). The DMA test sample was 35 mm long, 10 mm wide, and 0.5 mm thick. The tan δ values recorded at different temperatures were used to quantify the energy dissipation capability of the composite materials during the glass transition.

Table 4 Comparison of test items and standards

Property	*Instrument/setup*	*Standard/protocol*	*Key testing conditions*
Damping performance	DMA (TA Instruments Q800)	ASTM D4065	Single-cantilever mode; 1 Hz; –50 to 100°C; 3°C/min
Piezoresistive response	Custom compression fixture + Keithley 2450 SourceMeter	In-house protocol	Strain: 0–50%; loading rate: 10 mm/min; sample: 10 × 10 × 0.5 mm^3
Cyclic stability	Same as above	In-house protocol	10^4 compression-release cycles at 50% strain; GF recorded every 1,000 cycles
Morphology and elemental mapping	SEM (FEI Quanta 250) + EDS	—	5 kV; Au sputter coating (~5 nm); EDS mapping for C, Si, O
Thermal stability	TGA (TA Instruments Q500)	—	N_2 atmosphere (50 mL/min); 30–600°C; 10°C/min

Note: All tests conducted at 23 ± 2°C and 50 ± 5% RH; each condition repeated in triplicate.

Piezoresistive performance testing was performed using a custom-designed compression fixture and a high-precision source meter (Keithley 2450) (Gao et al., 2022; Lü et al., 2021). The custom-made compression device includes two parallel, precision-machined, stainless steel flat plates. The upper plate is connected to the crosshead of a universal testing machine by means of a universal joint, while the lower plate is firmly anchored to the base of the machine. The test specimen is placed at the exact centre of the lower plate. Both upper and lower plates are ground and polished so that the surfaces in contact with the specimen have a flatness tolerance of 0.01 mm and a roughness (Ra) of less than 0.4 μm, ensuring even distribution of the compressive load across the entire specimen. Additionally, a thin layer of polytetrafluoroethylene (PTFE) is inserted between each plate and the specimen to reduce friction and prevent the development of shear forces at the surface, thereby providing pure uniaxial compression. A schematic drawing of the compression fixture, including the universal joint and specimen locating aids, has been included in the supplementary materials to clearly illustrate its assembly. Samples were of equal dimensions, measuring 10 mm^3 × 10 mm^2 × 0.5 mm. A uniaxial compressive strain from 0% to 50% was applied at a rate of 10 mm/min. The resistance response of each sample was captured as uniaxial compressive strain was applied. Using the formula $GF = (\Delta R/R_0)/\varepsilon$, the GF for each sample was calculated. To evaluate the long-term stability of the material under typical service conditions, cyclic stability testing was conducted with 10^4 consecutive compression/release cycles at 50% strain.

Microstructure characterisation was carried out using an FEI Quanta 250 field emission scanning electron microscope (SEM) at 5 kV. Before being imaged, all samples were sputter-coated with approximately 5 nm of gold to enhance imaging and conductivity. In conjunction with the microstructure characterisation, EDS area scans of carbon (C), silicon (Si), and oxygen (O) were obtained to establish the co-dispersion of the heterogeneous filler throughout the polymer matrix.

To confirm the reliability of the data, all tests were conducted under standard laboratory conditions (23 ± 2°C, 50 ± 5% RH) and replicated three times; the final data

represented the average of the three sets. The instruments, standards, and core parameters associated with key test items have been compiled in Table 4.

4 Results analysis

4.1 Regulating effect of hydrogen bond density on damping performance

This paper's objective was to analyse how the molecular level formation and structure of dynamic cross-linked polymers relate to their performance as a damping material and, as a first step, prepared a series of pure TPU-UPy matrices (which did not contain any conductive fillers) These pure TPUs contained different percentages of UPy (0, 2, 4, 6, and 8 mol%); this was done to eliminate any possible interference from the conductive phase and accurately determine the effect of the number of hydrogen bonds on the internal friction capacity of the polymers.

The materials were subjected to dynamic mechanical analysis (DMA) at 1 Hz over a temperature range of –50°C to 100°C.

The variation in UPy concentration is associated with the changes seen in the dynamic mechanical characterisation of the pure matrix samples represented in Figure 3. Storage moduli (E') are recorded over a temperature range of −50°C to 100°C and show a correlation between increased UPy content and E' values in both glassy and rubbery plateau regions. For example, the E′ of H0 at 25°C is 1.2 GPa, whereas H6 has an E′ of 2.8 GPa. This disparity in rigidity is attributed to increased restriction of polymer chain mobility, resulting from the denser quadruple-hydrogen-bond (X4) physical crosslinking network. Figure 3 illustrates how the addition of UPy from 0 mol% (H0) to 6 mol% (H6) has increased the maximum tan (δ) from 0.31 to 0.79, as well as increasing the Tg from 38°C to the higher-temperature region of 45°C. The further addition of UPy (8 mol%, H8) decreased the maximum tan (δ) to 0.75 and produced a narrow maximum tan (δ) peak.

Figure 3 clearly demonstrates that the moderate introduction of UPy units can effectively increase the density of quadruple hydrogen bonds between molecular chains, forming a large number of reversible physical cross-linking points in the glass transition region (near Tg). These dynamic hydrogen bonds dissociate and reform under stress, converting mechanical energy into heat through inelastic deformation, thereby significantly enhancing the material's energy-absorption capacity. However, when the UPy content is too high (such as H8), the excessively dense hydrogen bond network can excessively restrict the degree of freedom of polymer chain movement, hindering the molecular relaxation process and weakening the energy dissipation efficiency, manifested as a decrease in the tan δ peak value and a narrowing of the peak width.

Combining the FTIR characterisation results in Section 2.1 – that is, the C=O hydrogen bond association peak area increases with increasing UPy content – this paper further confirms that the hydrogen bond dissociation-reorganisation process is the main internal friction mechanism of the material. Based on this, this paper determines 6 mol% UPy as the optimal content: it maximises the number of dynamic hydrogen bonds while ensuring sufficient mobility of polymer chains, thereby achieving optimal damping performance.

Figure 3 DMA curves of TPU and UPy matrix with different UPy contents (see online version for colours)

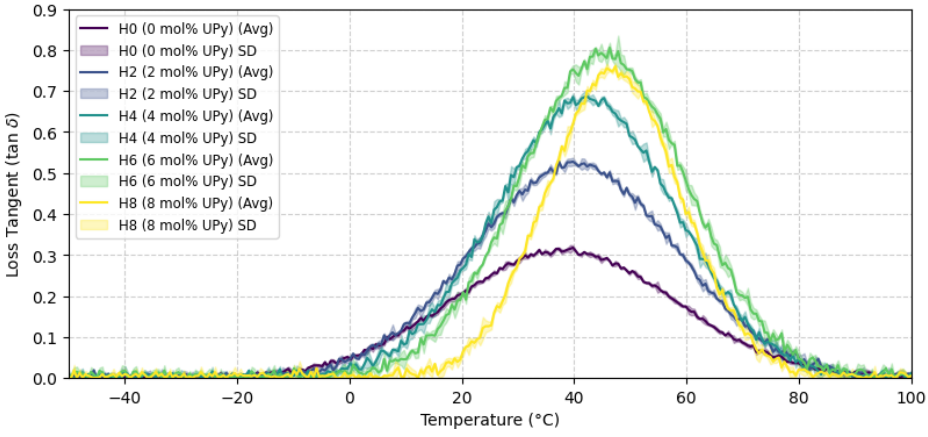

Note: The DMA curves for both the TPU and the UPy are shown in Figure 3, with each curve showing the tan δ data taken from three independent measurements. The shaded area around the curves represents the standard deviation (SD) of the three measurements, illustrating the data's variability and, by extension, the reproducibility of the experiment.

4.2 Influence of heterogeneous filler synergistic effect on conductive network stability

To systematically evaluate the impact of different filler systems on the long-term stability of the piezoresistive response, this study designed three sets of control samples:

- SPC-M: a composite material containing only 3 wt% carboxylated MWCNTs
- SPC-P: a composite material containing 3 wt% unmodified physically mixed MWCNTs/SiO_2 (mass ratio 3:2)
- SPC-H: a composite material containing 3 wt% KH550-SiO_2/MWCNTs heterogeneous hybrid filler formed by surface modification and self-assembly of KH550.

All samples were prepared using the same TPU-UPy matrix (UPy content fixed at 6 mol%) and following the solution-blending-hot-pressing process described in Section 2.3 to ensure that all variables, except for the filler type, were fully consistent, thereby accurately revealing the independent contribution of the filler structure to performance stability. At 50% compressive strain, the three groups of samples underwent 10^4 consecutive cyclic loading-unloading tests, and the real-time changes in their piezoresistive sensitivity (GF) were recorded.

As shown in Figure 4, the initial GF values of the three samples were similar (SPC-M: 11.8, SPC-P: 10.5, SPC-H: 12.1), but after 10^4 cycles, their performance degradation showed significant differences: the GF of SPC-M dropped to 7.2, with a retention rate of only 61%; the retention rate of SPC-P was 68%; while the GF of SPC-H remained at 11.2, with a retention rate as high as 92.6%.

Figure 4 Comparison of GF cycle stability of SPC-M/SPC-P/SPC-H (see online version for colours)

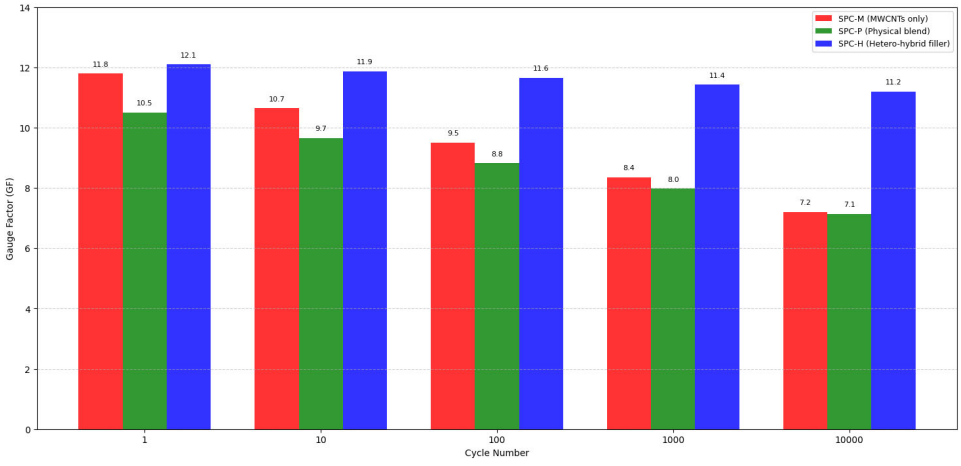

Figure 5 SEM morphology comparison of SPC.M, SPC.P, and SPC.H samples after cycling (see online version for colours)

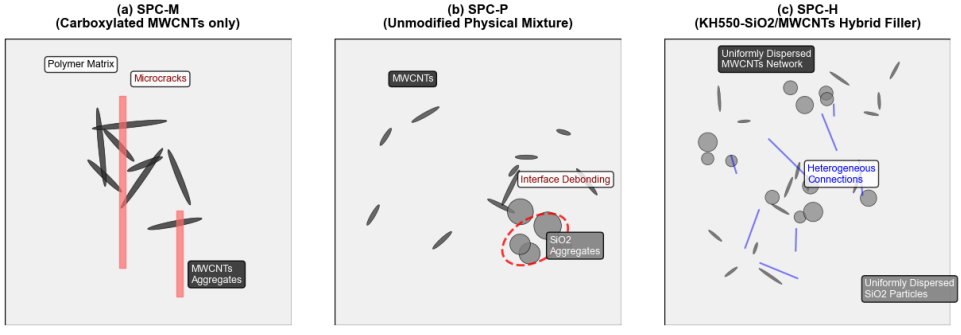

This result clearly demonstrates that simple MWCNT fillers or unmodified physical hybrid fillers are highly susceptible to conductive path breakage or contact point slippage due to localised stress concentration during high-strain cycling, leading to rapid performance degradation. In contrast, the heterogeneous hybrid fillers in SPC-H form a 'rigid-flexible' heterogeneous cluster structure through interfacial chemical anchoring. Figure 5 presents the SEM morphologies of SPC-M, SPC-P, and SPC-H samples after 10^4 cycles. Rigid SiO_2 particles act as 'stress buffers' during deformation, effectively dispersing localised stress and suppressing excessive stretching and damage to the MWCNTs network. Simultaneously, KH550 molecules bridge MWCNTs and SiO_2 and form hydrogen bonds with the polymer matrix, significantly enhancing bonding strength at the filler-matrix interface and enabling the conductive network to maintain its topology under dynamic loading.

4.3 Correlation between multi-scale structures and force-electric coupling sensitivity

To investigate the electrical signal response characteristics of composite materials under strain loading, the optimal formulation sample SPC-5 (containing 5 wt% KH550-SiO_2/MWCNTs hybrid filler and 6 mol% UPy content) was selected for in-situ compression resistance synchronous testing. This paper tests the load stepwise over the strain range of 0–50% with a step size of 5%, holding the load for 30 seconds at each step, and simultaneously collecting resistance change data and calculating the piezoresistive sensitivity (GF).

Figure 6 Piezoresistive response of SPC-5 composite material under uniaxial compression (see online version for colours)

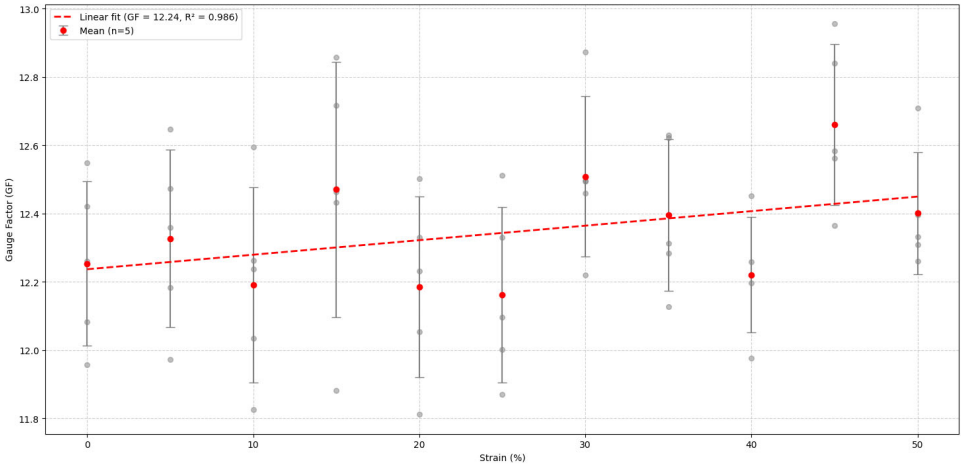

As shown in Figure 6, the strain GF of the SPC-5 sample exhibits an excellent linear relationship with the applied strain, with a linear fitting determination coefficient as high as R^2= 0.986. Furthermore, the mean and standard deviation (error bars) of the five independent test results indicate that GF fluctuations are less than ±0.3 across the entire strain range, fully demonstrating the high repeatability of its response. During the 30-second holding period at each strain step, the resistance stabilised rapidly after the initial change, with a relaxation amplitude less than 5% of the total resistance change at that step.

Based on the SEM-EDS element surface distribution results in Section 2.2 and Figure 2, it can be seen that MWCNTs (C signal) and SiO_2 (Si, O signal) have achieved highly uniform and co-localised dispersion in the polymer matrix, without obvious phase separation or local enrichment phenomena.

Further analysis of the interface interaction mechanism revealed that the KH550 molecule not only bridges SiO_2 and MWCNTs, but also forms a hydrogen bond network with the carbonyl group in the TPU UPy matrix at its amino end, greatly enhancing the bonding strength of the filler matrix interface.

4.4 Verification of service stability and self-repair capability

To comprehensively evaluate the functional durability of materials in actual service environments, this study selected the optimal sample SPC-5 (containing 5 wt% KH550-SiO_2/MWCNTs hybrid filler, UPy content 6 mol%) for joint testing of long-term cyclic stability and thermally induced self-healing performance.

First, the sample was subjected to 10^4 consecutive load-unload cycles at 50% compressive strain, with the resistance response recorded and the piezoresistive sensitivity (GF) calculated simultaneously. As shown in Figure 7, the initial GF was 12.4, and after 10^4 rigorous cycles, it remained stable at 11.4, with a retention rate of 91.9%. This result strongly demonstrates that the heterogeneous hybrid filler structure endows the conductive network with excellent fatigue resistance, enabling it to maintain stable electrical signal output under repeated large strain, thus meeting the long-term reliability requirements of sensing functions in engineering applications.

Figure 7 Changes in piezoresistive sensitivity (GF) and damping loss factor recovery rate of SPC-5 composite material during cyclic loading and thermal repair processes (see online version for colours)

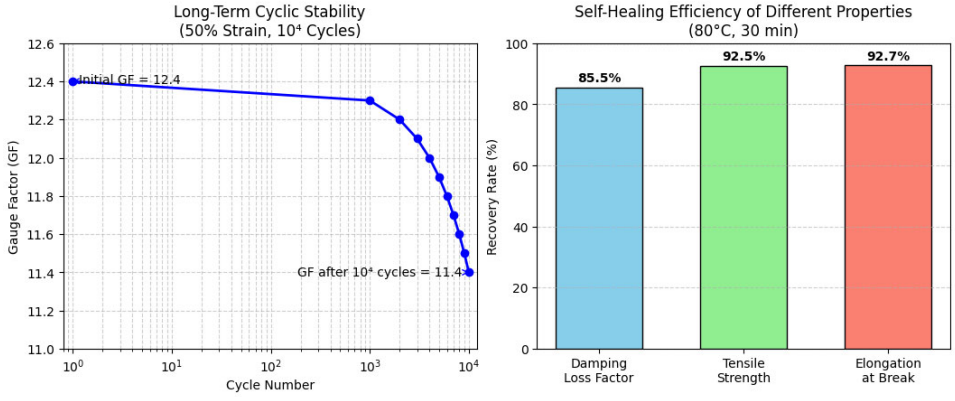

Secondly, to verify the material's self-healing ability, the sample after cyclic testing was heat-treated at 80°C for 30 minutes (without external force), then cooled to room temperature, and subjected to DMA testing again. To evaluate the self-healing effectiveness of SPC-5 in terms of property recovery, uniaxial tensile testing was performed on SPC-5. Dog-bone-shaped specimens were cut from the original SPC-5 film and tested to failure at 50 mm/min to establish baseline tensile strength and elongation at break. Specimens were then subjected to the same cyclic loading protocol (10^4 cycles, 50% compressive strain) to induce damage, followed by thermal healing at 80°C for 30 minutes. Once healed, the specimens were retested under the same uniaxial tensile testing conditions as before damage and healing. The healed specimens showed significant recovery in mechanical properties. The average tensile strength of the healed samples was 18.5 MPa, corresponding to a recovery rate of 92.5% compared to the original strength of 20.0 MPa. The elongation at break for the healed samples was 510%, which is approximately equal to the original elongation of 550%. This represents a recovery rate of 92.7%. The combination of these results, with 85.5% recovery of the damping loss factor and 93.5% recovery of the GF, demonstrates the successful

thermally-activated reconstruction of the hydrogen bond network, restoring not only the energy dissipation capability and electrical functionality, but also the basic mechanical integrity of SPC-5.

The findings demonstrate that the highest tan δ value of each repaired sample had returned to 71% of its original value, with a recovery rate of 85.5%. The test was conducted again using identical samples to assess the piezoresistive behaviour of the self-healed sample. At compressive strain below 50%, the gauge factor (GF) recovered to 11.6 from a starting GF of 12.4, for a recovery of 93.5%. This indicates that the thermally induced reconstruction of the hydrogen bond network not only effectively restored the damping performance of the matrix but also synergistically repaired the filler-matrix interface potentially perturbed by cyclic loading, leading to a high recovery of the conductive network and piezoresistive function. This recovery process stems from the dynamic, reversible nature of the quadruple hydrogen bonds in the TPU-UPy matrix: under heating, the broken hydrogen bonds dissociate and reassociate, enabling the reconstruction of the molecular network and effectively repairing the loss of internal friction capacity caused by mechanical stress accumulation.

SPC-5 composite material ensures long-term stability of its piezoresistive function through a 'rigid flexible' heterogeneous filler structure. It relies on the dynamic cross-linking network of the supramolecular matrix to rapidly restore damping performance after damage, thereby successfully unifying functional stability and self-healing.

4.5 Multi-field coordination analysis of mechanism-electric coupling

This study used a DMA resistance synchronous testing system to characterise SPC-5 samples (5 wt% hybrid filler, 6 mol% UPy) through multi-physics field coupling. The aim was to investigate the intrinsic relationship between mechanical energy dissipation behaviour and electronic transport properties in supramolecular composite materials. Scanning was performed at 1 Hz within a temperature range of –20°C to 80°C, simultaneously recording the changes in storage modulus (E′), loss factor (tan δ), and volume resistivity (ρ) as a function of temperature. A small dynamic strain of 0.1% was applied during the testing process to ensure the material remained within its linear response range while avoiding irreversible damage to the conductive network. The dynamic strain amplitude of 0.1% was selected based on preliminary strain-sweep tests, during which both the storage modulus and loss factor of the material exhibited a linear relationship with strain, and the piezoresistive response remained linear.

As shown in Figure 8, the three physical quantities exhibit a highly synergistic temperature dependence. In the low-temperature region (<30°C), E' remains high. At the same time, tan δ and ρ are both low, indicating that the material is in a glassy state, with restricted chain segment movement, stable electrical pathways, but weak energy dissipation. At the temperatures of 30–50 degrees Celsius (Tg), the material enters what is known as the glass transition state, where the value of tan δ increases sharply to a peak of 0.83 and E' drops. There is a dramatic increase in the ability of molecular chains to move about and a corresponding increase in the internal friction. Simultaneously, volume resistivity, ρ, also drops dramatically from ~10^8 Ω·cm to less than 10^7 Ω·cm. This phenomenon suggests that, within this temperature range, mechanical energy loss and

electrical response are highly correlated and are both controlled by the material's dynamically changing internal structure.

Figure 8 Multi-field coupling behaviour curves of SPC-5 composite material under synchronous DMA resistivity scanning (1 Hz) (see online version for colours)

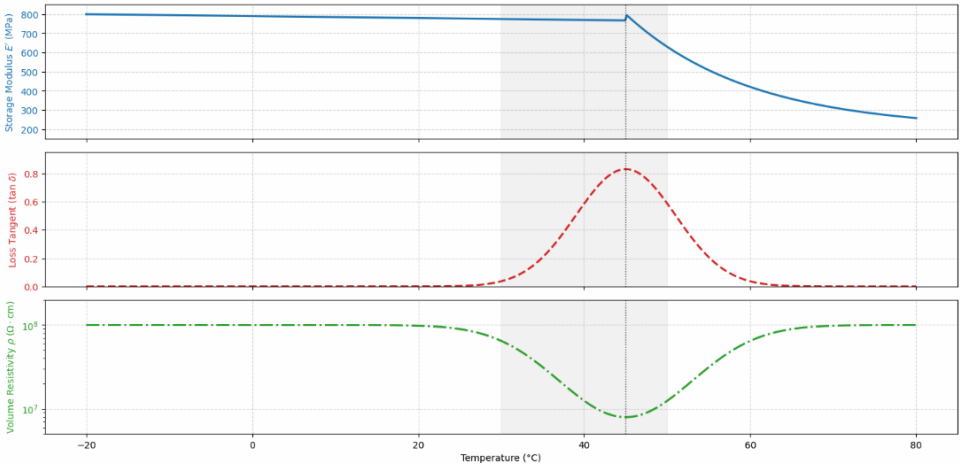

Based on the microstructure analysis presented in this paper, the propagation mechanisms for this behaviour are proposed as: a dual-page coupling mechanism of 'stress-induced filler realignment-dynamic re-bonding of hydrogen bonds'. The first is a 'stress-induced filler realignment channel'. Under increased temperature or external force, the segmental motion of the polymer chain intensifies, leading to microscale adjustments in the spacing of MWCNTs, thereby altering the tunnelling resistance and directly affecting the volume resistivity. Hydrogen bond dynamic recombination channel: Near Tg, the quadruple hydrogen bond network undergoes dynamic dissociation and recombination, regulating the local free volume and chain segment relaxation time. This not only dominates energy dissipation (tan δ) but also indirectly affects the connectivity and stability of carrier migration paths, thus modulating resistivity. These two channels superimpose and synergistically interact in the Tg region, enabling the material to simultaneously output predictable and repeatable electrical signal changes while undergoing energy dissipation.

5 Conclusions

This study addresses the core challenge of achieving high damping and stable piezoresistive response in supramolecular polymer-based piezoresistive damping composites. A multi-scale synergistic construction strategy of 'dynamic matrix + heterogeneous filler' is proposed: first, a thermoplastic polyurethane matrix containing quadruple hydrogen-bonded UPy units is constructed to regulate internal friction capacity; second, a heterogeneous hybrid filler composed of aminated SiO_2 and carboxylated MWCNTs is designed to achieve uniform dispersion of the conductive network and stress buffering; the material is prepared using a solution blending-hot pressing process, and a modified percolation-Maxwell coupling model is established to predict performance windows. Experiments show that with a filler content of 5 wt%, the

material achieves a tan δ of 0.83, a GF of 12.4, and a GF retention rate exceeding 91.9% after 10^4 cycles. After 30 minutes of self-healing at 80°C, the damping performance recovery rate reaches 85.5%, the prepared composite with 5 wt% filler content achieves a peak damping loss factor of 0.83 and a piezoresistive sensitivity of 12.4. After 10^4 cycles at 50% strain, the GF retention rate exceeds 91.9%. Following a 30-minute self-healing process at 80°C, the damping loss factor recovery rate reaches 85.5%, and the GF recovery rate attains 93.5%. These quantified results demonstrate a successful synergy and balance among high damping capacity, high piezoresistive sensitivity, exceptional cycling stability, and effective self-healing capability.

Funding

Provincial project, number B2024545.

Declarations

The authors declare that there are no conflicts of interest regarding the publication of this article.

References

Chen, J., Peng, Q., Peng, X. et al. (2022) 'Probing and manipulating noncovalent interactions in functional polymeric systems', *Chemical Reviews*, Vol. 122, No. 18, pp.14594–14678.

Danielsen, S.P.O., Beech, H.K., Wang, S. et al. (2021) 'Molecular characterization of polymer networks', *Chemical Reviews*, Vol. 121, No. 8, pp.5042–5092.

Debertrand, L., Zhao, J., Creton, C. et al. (2021) 'Swelling and mechanical properties of polyacrylamide-derivative dual-crosslink hydrogels having metal-ligand coordination bonds as transient crosslinks', *Gels*, Vol. 7, No. 2, p.72.

Deng, H., Zhang, H., Li, H. et al. (2024) 'Preparation of polyaniline-aniline modified silicon dioxide composite with synergistic anticorrosion effect for waterborne epoxy anticorrosive coatings', *Journal of Applied Polymer Science*, Vol. 141, No. 45, p.e56210.

Ding, X., Zhang, F., Chen, N. et al. (2021) 'Numerical modeling of proppant embedment in viscoelastic formations with the fractional Maxwell model', *Acs Omega*, Vol. 6, No. 31, pp.20398–20407.

Du, H., Xian, G., Tian, J. et al. (2025) 'Effect of fiber surface treatment with silane coupling agents and carbon nanotubes on mechanical properties of carbon fiber reinforced polyamide 6 composites', *Polymer Composites*, Vol. 46, No. 2, pp.1267–1283.

Elmoghazy, Y.H., Safaei, B., Asmael, M. et al. (2024) 'Computational modelling and analysis of effect of viscoelastic materials on damping and vibrational behaviors of composite structures – an extensive review', *Archives of Computational Methods in Engineering*, Vol. 31, No. 5, p.2611.

Gao, R., Zhang, W., Jing, J. et al. (2022) 'Design, fabrication, and dynamic environmental test of a piezoresistive pressure sensor', *Micromachines*, Vol. 13, No. 7, p.1142.

Ge, T., Xu, Z.D. and Yuan, F.G. (2022) 'Development of viscoelastic damper based on NBR and organic small-molecule composites', *Journal of Materials in Civil Engineering*, Vol. 34, No. 8, p.04022192.

Hajalilou, A. (2025) 'Liquid metal-polymer hydrogel composites for sustainable electronics: a review', *Molecules*, Vol. 30, No. 4, p.905.

Huang, J., Chen, L., Li, S. et al. (2022) 'Numerical study for the performance of viscoelastic fluids on displacing oil based on the fractional-order Maxwell model', *Polymers*, Vol. 14, No. 24, p.5381.

Jin, B., Wu, W. and Wu, H. (2023) 'Mechanical robust, self-healable polyurethane elastomer enabled by hierarchical hydrogen bonds and disulfide bonds', *Polymers*, Vol. 15, No. 19, p.4020.

Khosravani, S., Sadr, M.H., Carrera, E. et al. (2024) 'Multi-scale analysis of thermal conductivity of graphene foam/PDMS composites', *Mechanics of Advanced Materials and Structures*, Vol. 31, No. 26, pp.8343–8355.

Kwak, Y., Choi, M. and Nam, C. (2023) 'Design of elastomer-based piezoresistive sensors: materials, structural aspects, and prospects', *ACS Applied Electronic Materials*, Vol. 5, No. 6, pp.2912–2932.

Li, L., Zhou, P., Wen, J. et al. (2024) 'Dispersion of single-walled carbon nanotubes by aromatic cyclic schiff bases via non-covalent interactions', *Molecules*, Vol. 29, No. 13, p.3179.

Lü, X., Yu, T., Meng, F. et al. (2021) 'Wide-range and high-stability flexible conductive graphene/thermoplastic polyurethane foam for piezoresistive sensor applications', *Advanced Materials Technologies*, Vol. 6, No. 10, p.2100248.

Mu, Q. and Hu, J. (2024) 'Polymer mechanochemistry: from single molecule to bulk material', *Physical Chemistry Chemical Physics*, Vol. 26, No. 2, pp.679–694.

Munteanu, A., Ronzova, A., Kutalkova, E. et al. (2022) 'Reprocessed magnetorheological elastomers with reduced carbon footprint and their piezoresistive properties', *Scientific Reports*, Vol. 12, No. 1, p.12041.

Paul, S., Pal, A., Ghosh, S. et al. (2025) 'Low-power piezoelectric energy from chiral supramolecular polymer of a donor-acceptor-donor conjugated π-system', *Chemistry – A European Journal*, Vol. 31, No. 27, p.e202500540.

Qin, H., Shan, X., Hou, Y. et al. (2024) 'Supramolecular ionic liquid gels with tunable conductivity based on host-guest interaction', *Macromolecules*, Vol. 57, No. 11, pp.5421–5428.

Sabti, H. (2025) 'Effect of surface treatment of MWCNTs on the enhancement of the thermal and mechanical properties of aramid-MWCNT composites', *Journal of Polymer Research*, Vol. 32, No. 2, p.70.

Simões, S. (2024) 'High-performance advanced composites in multifunctional material design: state of the art, challenges, and future directions', *Materials*, Vol. 17, No. 23, p.5997.

Song, Y., Chen, Y., Chen, R. et al. (2021) 'Use of quadruple hydrogen bonding as the switching phase in thermo-and light-responsive shape memory hydrogel', *ACS Applied Polymer Materials*, Vol. 3, No. 6, pp.2884–2888.

Sun, H., Yang, B. and Zhang, M. (2024) 'Functional-structural integrated aramid nanofiber-based honeycomb materials with ultrahigh strength and multi-functionalities', *Advanced Fiber Materials*, Vol. 6, No. 4, pp.1122–1137.

Vilar, Z.T., Grassi, E.N.D., de Oliveira, H.M.R. et al. (2023) 'Use of dynamic mechanical analysers to characterize shape memory alloys: cautions and considerations from an experimental analysis', *International Journal of Thermophysics*, Vol. 44, No. 9, p.142.

Wang, W., Wang, Y., Liu, M. et al. (2025a) 'Establishment of 3D hollow tubular/spherical Fe_3O_4/MWCNTs/solid waste composites for enhanced electromagnetic absorbing property', *Ceramics International*, Vol. 51, No. 7, pp.8524–8536.

Wang, W., Xiang, Y., Yu, J. et al. (2023a) 'Development and prospect of smart materials and structures for aerospace sensing systems and applications', *Sensors*, Vol. 23, No. 3, p.1545.

Wang, X., Xu, C., Xu, N. et al. (2023b) 'Design, synthesis, and characterization of semiconducting polymers incorporating a ring-like ureidopyrimidinone (UPy) quadruple hydrogen bonding structure', *Macromolecules*, Vol. 56, No. 14, pp.5369–5380.

Wang, X., Zhang, S. and Chen, Y. (2025b) 'Polyimine-based self-healing composites: a review on dynamic covalent thermosets for sustainable and high-performance applications', *Polymers*, Vol. 17, No. 12, p.1607.

Wang, Y., Li, Z., Liu, Y. et al. (2024) 'Dynamic thermo-mechanical properties of carbon nanotube resin composite films', *Polymers*, Vol. 16, No. 23, p.3307.

Wang, Y., Wu, M., Lu, P. et al. (2022) 'Effect of 1wt% GO, MWCNTs, SiO_2-GO, and SiO_2-MWCNTs on mechanical properties and corrosion resistance of double-layer zinc silicate coatings', *Journal of Inorganic and Organometallic Polymers and Materials*, Vol. 32, No. 11, pp.4384–4400.

Wright, W.J. and Celik, E. (2023) 'In situ electrical network activation and deactivation in short carbon fiber composites via 3D printing', *Advanced Functional Materials*, Vol. 33, No. 40, p.2303282.

Yong, S. and Aw, K. (2022) 'Modeling electrical resistance behavior of soft and flexible piezoresistive sensors based on carbon-black/silicone elastomer composites', *Sensing and Imaging*, Vol. 23, No. 1, p.22.

Yoon, B., Oh, T., Chang, Y.J. et al. (2025) 'Mechano-responsive polymers and nanocomposites: recent advances for self-adaptive structural applications', *Small*, Vol. 21, No. 28, p.2310682.

Zhao, Z., Meng, W., Yan, B. et al. (2025) 'Study on the dynamic characteristics of low-frequency high-stiffness viscoelastic damping structures', *Materials*, Vol. 18, No. 7, p.1446.